Desalination and Water Treatment
www.deswater.com
doi: 10.1080/19443994.2014.976275

57 (2016) 1647–1658
January

Taylor & Francis
Taylor & Francis Group

Application of generic cubic equations of state in the CFD simulation of the sweeping gas polytetrafluoroethylene (PTFE) membrane distillation

Pooya Jafari[a], Mostafa Keshavarz Moraveji[b,*]

[a]*Department of Civil and Environmental Engineering, University of Houston, 4800 Calhoun, Houston, TX 77204-4003, USA, Tel. +1 8329706016; email: pjafari@uh.edu*
[b]*Department of Chemical Engineering, Amirkabir University of Technology (Tehran Polytechnic), Hafez Ave, P.O. Box 15875-4413 Tehran, Iran, Tel. +98 9363098063; email: moraveji@aut.ac.ir*

Received 20 April 2014; Accepted 2 October 2014

ABSTRACT

Sweeping gas membrane distillation is one of the membrane separation processes which has many applications in industries such as desalination and water purification. In this work, computational fluid dynamics has been used to model and simulate the momentum and mass transfers in the sweeping gas polytetrafluoroethylene membrane distillation. Three generic cubic equations of state have been used to make a connection between the water concentrations in the liquid and gas phase adjacent to the membrane. The validity of the three proposed cubic equations including Peng–Robison, Redlich–Kwong, and Soave–Redlich–Kwong have been obtained and the results have shown that the best among them in fitting with the experimental results is Peng–Robison. Effect of different operating conditions on the permeate flux such as feed temperature, concentration, flow rate, and sweeping gas flow rate has been examined. The rise in the feed temperature, flow rate and sweeping gas flow rate results in mass transfer driving force increase and permeate flux increase in both of experimental and simulated results. The simulated results show that the effect of feed concentration increase is negligible for the modeled results, while it has a negative effect in the experimental results due to the membrane fouling and temperature polarization.

Keywords: Sweeping gas membrane distillation (SGMD); CFD; Polytetrafluoroethylene (PTFE); Equations of State

1. Introduction

Membrane distillation (MD) is a relatively new membrane separation process in which vapor molecules pass through it due to its hydrophobia nature. Difference in vapor pressure between feed and permeate side of the membrane provides the MD driving force needed for the transport of the permeant through the membrane. MD has many applications in the desalination of salty water due to the water shortage in the world, chemical industries where azeotropic distillation is costly, biomedical and pharmaceutical industries, and food industries in which concentration of different juices or milk is aimed. MD can be coupled with the other separation processes such as distillation, ultrafiltration, and nanofiltration which can result in higher proficiencies of the hybrid system.

*Corresponding author.

However, the MD has some drawbacks that keep it away from scaling it up from laboratorial scale into the large industrial scale. The main barriers are relative low permeability in comparison with other separation processes and, concentration and temperature polarization effects that can reduce the permeate flux. There are four common MD configurations: direct contact membrane distillation (DCMD), air gap membrane distillation, sweeping gas membrane distillation (SGMD), and vacuum membrane distillation (VMD) out of which the DCMD is the most studied configuration and the SGMD is the least studied one, because condensation of the vapor in the membrane module makes the process simple and omit the condensation step which is usually done by condenser or cold trap in the VMD and SGMD [1–3].

There are many proposed models for simulating the mass transport in the membranes. Solution–Diffusion is usually used for the nonporous membranes like the pervaporative membranes or the other asymmetric membranes in which the affinity between the feed and membrane materials is high. Solution–Diffusion–Evaporation is a common model in the separation of the gasses or in the dilute liquid solutions. However, there are three common models for the transport of the gas molecules through the porous membranes, for example, in the MD, named Knudsen flow, Poiseuille flow, and molecular diffusion in which the collision between molecules and wall's pores specifies its kind.

Computational fluid dynamics (CFD) is one of the approaches which have been used widely to simulate the momentum, heat, and mass transport in a diverse range of membranes. Continuity equations are derived and solved simultaneously in this method. The key factor in the modeling of the boundary layer sticking to the membrane is the relation between the concentrations of the permeant in the membrane's boundaries. Shirazian et al. [4–6] used the physical solubility of the permeant in the absorbent to relate the concentrations discussed above by membrane contactors. Rezakarami et al. [7] calculated the partition coefficient to relate the concentration of the water in both sides of the membrane in the water removal from water/ethylene glycol mixture.

Cubic equations of state are polynomial equations that are cubic in molar volume and are good balance between the simplicity and generality which makes them appropriate to many purposes. They are capable of representing the liquid and vapor behavior in a wide range of temperatures and pressures. Many generic cubic equations of states have been proposed after the arrival of van der Waals (vdW) equation of state in 1873. The most famous ones are Redlich–Kwong (RK), Soave–Redlich–Kwong (SRK), and Peng–Robison (PR), chronologically. In this study, we have used the generic cubic equations of state to build a relation between the permeant concentration in the liquid bulk phase adjacent to the membrane and its concentration in the gas state adjacent to the membrane. We have studied the separation of water from glucose syrup by SGMD with CFD, and the effects of feed temperature, feed concentration, feed flow rate, and sweeping gas flow rate on the Polytetrafluoroethylene (PTFE) membrane's performance have been modeled and compared with the experimental results. Peng–Robinson equation of state was the most powerful equation in fitting the experimental results among the three studied equations. The modeled and simulated permeate fluxes increase as temperature goes higher based on the Antoine equation, and the permeate flux plots vs. feed and sweep gas flow rates have similar ascending trends. Additionally, the validity of the RK, SRK, and PR cubic equations of states has been examined and the best equation has been found due to the minimum deviance with the experimental data.

2. Model development

In order to simulate the performance of the membrane in various conditions of different feed temperatures, feed concentrations, feed flow rates, and sweeping gas flow rates, we take the narrow element that contains membrane and both sides of the module as is shown in Fig. 1. Now, we can derive conservation equations by solving mass and momentum balance over the element. As it can be seen, the flow of glucose solution enters the element from the left side and exits from the right side of the feed section. At the permeate section, sweeping gas enters through the right side and exits from the left side. The membrane is closed from the left and the right side of the element.

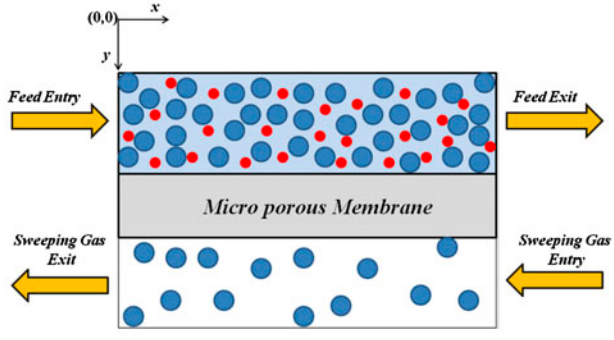

Fig. 1. An element contains feed, membrane, and permeate.

If we apply the law of mass conservation for the water in the element, we can get the equation of continuity that describes the transfer of water from the feed side to the permeate side. The equation of continuity for water describes the change in mass concentration of water with time at a fixed point in space by the diffusion and convection of water, as well as chemical reactions that produce or consumes water, and the differential form of this equation based on molar units may be written as [8]:

$$\frac{\partial C_W}{\partial t} = -(\nabla \cdot C_W V) - (\nabla \cdot J_W) + R_W \tag{1}$$

where C_W represents water concentration (mol/m^3), t represents time (s), R_W represents chemical reaction (mol/m^3 s), J_W is diffusive molar flux (mol/m^2 s) of the water species and can be written by Fick's law of diffusion as:

$$J_W = -D_W \nabla C_W \tag{2}$$

Here, D_W represents diffusion coefficient (m^2/s), V represents velocity vector (m/s) that can be obtained by coupling and solving mass and momentum conservation equations simultaneously. With this method, concentration and velocity distribution are achieved although the velocity distribution can be obtained analytically. Momentum equation with constant density and kinematic viscosity (viscous fluid) is called Navier–Stokes equation and may be written as [8]:

$$\rho\left(\frac{\partial V_y}{\partial t} + V_y \cdot \nabla V_y\right) = -\nabla P + \nabla \cdot (\mu \cdot (\nabla V_y + (\nabla V_y)^T)) + \rho g \tag{3}$$

Here, ρ is density (kg/m^3), P is pressure (Pa), μ is dynamic viscosity (Pa s), and g is gravity (m/s^2).

2.1. Assumptions

The modeling development is based on some assumptions which we have listed them below:

(1) Steady state and isothermal conditions for each temperature used in the experimental work.
(2) Laminar flow for the feed in the membrane module that is an acceptable assumption because of the low Reynolds number.
(3) Vapor/Liquid equilibrium at the interface of the feed and membrane [9].
(4) Only water penetrates through the membrane and the glucose remains in the feed section because 100% selectivity has achieved in experimental work [10].
(5) The decline in the solution's vapor pressure due to its glucose concentration is negligible because of its low quantity.

2.2. Feed section's equations and its boundary conditions

In the case of steady state and no reaction, the continuity equation for species water in the feed section is shortened to:

$$D_W\left(\frac{\partial^2 C_{Wf}}{\partial x^2} + \frac{\partial^2 C_{Wf}}{\partial y^2}\right) = V_y \frac{\partial C_{Wf}}{\partial y} \tag{4}$$

Here, C_{Wf} represents water concentration in the feed section (mol/m^3), D_W is estimated from Wilke–Chang correlation that is one of the most widely used, and it is an empirical modification of the Stokes–Einstein equation [11]. The boundary conditions for continuity and Navier–Stokes equations are:

$$\begin{aligned} &\text{At } y = 0, C_{Wf} = C_0, \\ &V_y = V_0(\text{inlet concentration, inlet velocity}) \end{aligned} \tag{5}$$

$$\text{At } y = L, \text{ convective flux}, P = P_{\text{out}} \tag{6}$$

The convective flux condition assumes only convection flux and no diffusion flux passes through the mentioned boundary.

$$\begin{aligned} &\text{At } x = 0, \frac{\partial C_{Wf}}{\partial y} = 0, \\ &V_y = 0 \,(\text{insulation/symmetry,no slip condition}) \end{aligned} \tag{7}$$

$$\begin{aligned} &\text{At } x = d_1, \\ &C_{Wf} = C_{Wm} \times \lambda, \\ &V_y = 0 \,(\text{insulation boundary/symmetry,} \\ &\qquad \text{no slip condition}) \end{aligned} \tag{8}$$

C_{Wm} represents vapor concentration in the membrane section (mol/m^3) and λ is a constant that relates the concentrations of water in the feed and membrane sections, this proportion of concentrations is estimated

from the proportion of $\frac{Z_v}{Z_l}$ in which Z_l and Z_v are compressibility factors of water in the liquid and vapor phases, respectively. It should be mentioned that water in the membrane is in gas state [9]. In order to calculate these quantities, vapor and vapor-like and liquid and liquid-like roots of the generic cubic equation of state are used. Cubic equations of state are called such, because they can be rewritten as a cubic function of v, molar volume (m^3/mol). These equations for Z are equivalent to [12]:

$$Z = 1 + \beta - q\beta\frac{Z-\beta}{(Z+\varepsilon\beta)(Z+\sigma\beta)} \tag{9}$$

(vapor and vapor-like roots of the generic cubic equation)

$$Z = \beta + (Z+\varepsilon\beta)(Z+\sigma\beta)\left(\frac{1+\beta-Z}{q\beta}\right) \tag{10}$$

(liquid and liquid-like roots of the generic cubic equation)

B and q are dimensionless constants that are estimated below as:

$$\beta = \Omega\frac{P_r}{T_r} \tag{11}$$

$$q = \frac{\Psi\alpha(T_r)}{\Omega T_r} \tag{12}$$

where P_r and T_r are reduced pressure and reduced temperature, respectively. ε, σ, Ω, and Ψ are other dimensionless constants whose quantities are related to those equations of states in which they are used. $\alpha(T_r)$ can be calculated as a function of the acentric factor (ω) and reduced temperature (T_r) as variables for the SRK and PR cubic equations of state whose functions are as below [12], while $\alpha(T_r)$ is a function of T_r for RK.

$$\alpha_{SRK}(T_r;\omega) = [1 + (0.480 + 1.574\omega - 0.176\omega^2)(1 - {T_r}^{1/2})]^2 \tag{13}$$

$$\alpha_{PR}(T_r;\omega) = [1 + (0.37464 + 1.54226\omega - 0.26992\omega^2)(1 - {T_r}^{1/2})]^2 \tag{14}$$

$$\alpha_{RK}(T_r) = T_r^{-1/2} \tag{15}$$

The molar volume for each liquid and gas phase is obtained by substituting Z from each of above Eqs. (9) and (10) into the below equation:

$$v = \frac{ZRT}{P} \tag{16}$$

where T is the temperature (K); if we assume v_l and v_g as molar volumes of water in the liquid and gas phase (m^3/mol), the proportion of $\frac{v_g}{v_l}$ will be equal to λ and satisfies its boundary condition.

The dynamic viscosity (μ) of glucose solution in the feed section is calculated from a proposed analytical relationship by Converti et al. [13]:

$$\mu = A_W \exp\left(\frac{B_W}{T}\right) + C_G A_G \exp\left(\frac{B_G}{T}\right) \tag{17}$$

Here, A_W and A_G are dimensional quantities for water and glucose (g/m s and m^2/s), respectively. B_W and B_G are some other quantities for water and glucose in Kelvin. Eq. (17) has been achieved by empirical relationship that has been widely used to quantify the effect of temperature on the dynamic viscosity [14].

2.3. Membrane section's equations and its boundary conditions

In the membrane section, only the equation of continuity is applied. The continuity equation in the case of steady state, no reaction and no convective flux through the membrane is shortened to:

$$D_W\left(\frac{\partial^2 C_{Wm}}{\partial x^2} + \frac{\partial^2 C_{Wm}}{\partial y^2}\right) = 0 \tag{18}$$

For estimating D_W, the most dominant factor is Knudsen number, which is a dimensionless number defined as the proportion of mean free path length to a representative physical length scale. The Knudsen diffusion is important when the Knudsen number reaches the quantity of one. Knudsen number always is for situations where the mean free path of molecules is greater than the pore size, so molecules collide with the wall frequently [15]. Knudsen applies to gases rather than liquids, because the liquid molecules are very close to each other. In this work with the Knudsen number of almost one, the Knudsen diffusion is used to estimate the diffusion coefficient in the membrane section.

The boundary conditions for continuity equation are:

$$\text{At } y = 0, \frac{\partial C_{Wm}}{\partial y} = 0 \text{ (insulation/symmetry)} \quad (19)$$

$$\text{At } y = L, \frac{\partial C_{Wm}}{\partial y} = 0 \text{ (insulation/symmetry)} \quad (20)$$

$$\text{At } x = d_1, C_{Wm} = \frac{C_{Wf}}{\lambda} \text{(concentration)} \quad (21)$$

$$\text{At } x = d_2, C_{Wm} = \frac{C_{Wp}}{\lambda} \text{(concentration)} \quad (22)$$

Here, C_{Wp} is vapor concentration in the permeate section (mol/m^3).

2.4. Permeate section equation and its boundary conditions

In the case of steady state and no reaction, the continuity equation for species water in the feed section is shortened to:

$$D_W \left(\frac{\partial^2 C_{Wp}}{\partial x^2} + \frac{\partial^2 C_{Wp}}{\partial y^2} \right) = V_y \frac{\partial C_{Wp}}{\partial y} \quad (23)$$

D_W can be estimated by Chapman–Enskog theory in which its inherent assumptions are quite restrictive (i.e. low density and spherical atoms), and its intrinsic potential function is empirical. Despite that, it provides good estimates of diffusion coefficient for many polyatomic gases and gas mixtures [11].

The boundary conditions for continuity equation are:

$$\text{At } y = 0, \text{ convective flux} \quad (24)$$

$$\text{At } y = L, C_{\text{wp}} = 0 \quad (25)$$

$$\text{At } x = d_2, C_{wp} = C_{Wm} \text{ (concentration)} \quad (26)$$

$$\text{At } x = d_3, \frac{\partial C_{Wp}}{\partial y} = 0 \text{ (insulation/symmetry)} \quad (27)$$

2.5. Numerical solution for conservation equations (continuity and momentum equations)

The conservation equations which were derived above are solved numerically for each three sections (feed, membrane, and permeate) in the two dimensions (x and y) by COMSOL Multiphysics Software version 4.3.2. COMSOL Multiphysics uses the proven finite element method (FEM). The software runs the finite element analysis together with adaptive meshing and error control using a variety of numerical solvers. One of these solvers is UMFPACK, a highly efficient direct solver for nonsymmetric systems. Suitability and validity of this solver has been proved and shown in some literature [7,10]. For a two-dimensional geometry, it is optional between creating a free mesh consisting of triangular elements, a free mesh consisting of quadrilateral elements, or a mapped mesh consisting of quadrilateral elements. Triangular mesh is used in this work and mesh element sizes are controlled near the membrane edge to have more accurate distribution, and the regular refinement method is used to divide each element into four triangular elements. This generates an anisotropic mesh with 3,776 elements (Fig. 2). For triangular elements, COMSOL Multiphysics computes the mesh quality q as:

$$q = \frac{4\sqrt{3}}{h_1^2 + h_2^2 + h_3^2} A \quad (28)$$

where A is the area, and h_1, h_2, and h_3 are the side lengths of the triangle. The value of q is a number between 0 and 1. If $q > 0.3$, the mesh quality should not affect the solution's quality. Mesh quality of current simulation is 0.8459 and quarantines that there are no disruptions from mesh quality in the solution's quality. Computational time for solving the set of equations is about 2 min by means of An intel(R) Core™ i7 (CPU speed of 1.73 GHz and 4 GB of RAM).

3. Result and discussion

3.1. The validity of the generic cubic equations of state

Here, the equation with the best ability to match with the experimental results is required. This equation should be capable of modeling the vapor–liquid equilibrium at the feed–membrane interface with the least deviation from the experimental results. Each of the cubic equations of state including RK, SRK, and PR has been studied for this study and their parameter assignments have been summarized in Table 1.

In order to relate the concentration of water in liquid phase at the feed–membrane interface to the concentration of vapor in the membrane at the feed–membrane interface which penetrates through the

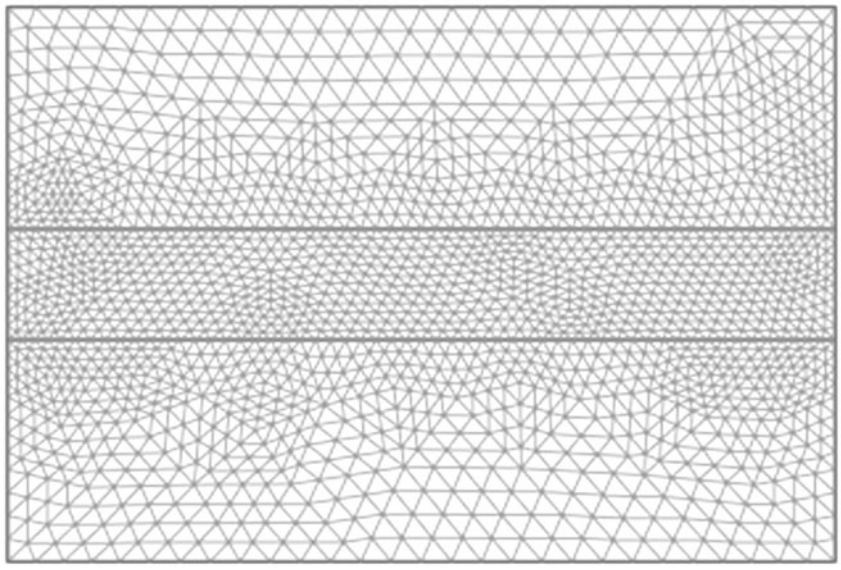

Fig. 2. Meshing used by finite element for analysis.

Table 1
Parameter assignments for equations of state (55°C) [12]

Cubic equations of state	$\alpha(T_r)$	σ	ε	Ω	Ψ	Z_c
RK	1.40462	1	0	0.08664	0.42748	1/3
SRK	1.65850	1	0	0.08664	0.42748	1/3
PR	1.56540	$1+\sqrt{2}$	$1-\sqrt{2}$	0.07780	0.45724	0.30740

micro porous membrane, we should have the quantity of λ. The values of compressibility factors of water in the liquid and gas phases that yield an estimation of λ for each of the generic cubic equations of state and calculated flux for each of these equations under the constant conditions have been summarized in Table 2.

This table predicts that the difference between the concentration of liquid water and vapor will be more based on the PR equation and the decline in the concentration profile will be sharper based on this equation, while the concentration profiles achieved from RK and SRK are more similar to each other. The concentration profile for the permeant in the feed, membrane, and permeate section has been modeled and its result has been given in Fig. 3 for each of the utilized cubic equations of state. It is obvious from these plots that water concentration is more in the feed section and less in the permeate section as water is in the liquid phase in the feed section and in the gas phase in the membrane section. Permeate flux modeled by PR is lower than the other two fluxes which is obtained when modeled by the SRK and RK. The comparison between the equations of state and experimental results show that these equations are capable of modeling the membrane performance to some extent. At present, there is no equations of state that can predict accurately the equilibrium properties of water in gas and liquid phase under all conditions and these equations can be

Table 2
The liquid and gas compressibility factors and their ratio, and permeate flux (30 g/l, 55°C, 400 ml/min, and 10 SCFH)

Cubic equations of state	Z_l	Z_v	λ	Flux (L/m^2h)
RK	1.48695×10^{-4}	0.998445	6,714.718047	8.719
SRK	1.43260×10^{-4}	0.998141	6,967.339104	8.747
PR	1.25981×10^{-4}	0.998110	7,922.702630	7.539
Experimental				5.9

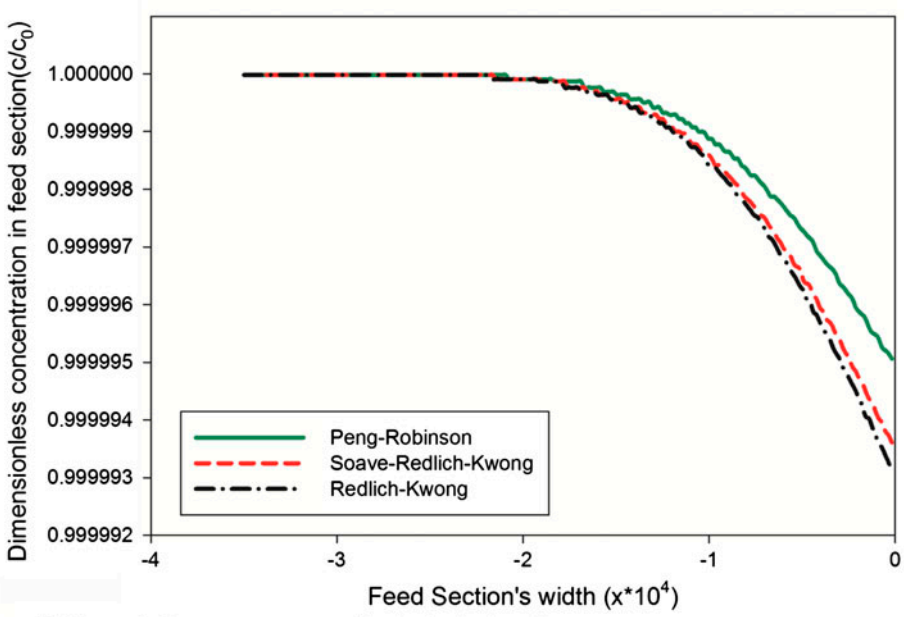

(a) Dimensionless water concentration in the feed section

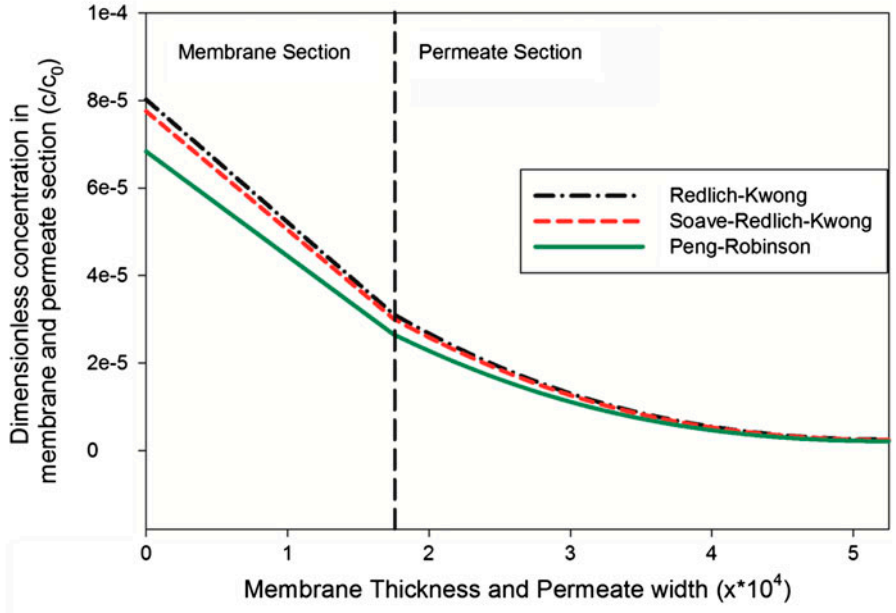

(b) Dimensionless water concentration in the Membrane and Permeate section

Fig. 3. Permeant concentration profile in the feed (a) and membrane and permeate sections (b).

used to have the appropriate prediction of the results and its criteria under the mentioned operating conditions. So, using these cubic equations, we can have good approximates of experimental results in the MDs whose major uses are in desalination and water purification. The difference between the experimental and simulated results can be related to the temperature drop along the membrane module, which is occurred by evaporative cooling at the permeate side [16]. The temperature drop yields to the exponential flux decline according to the Antoine equation.

Fig. 4 shows the arrow plot of the permeant flux in the studied domain. The mass transfer in the feed and permeate section includes both diffusion and convection, while diffusion dominates the mass transfer in the porous membrane. The flux arrow is uniform in

the feed and membrane sections as both of them are isolated from left to right, and up and down, respectively. Flux in the permeate section is two dimensional, because of the permeant flux and the sweep gas velocity that are at different dimensions.

3.2. Effect of feed temperature

According to the Antoine equation, the increase in the feed temperature will enhance the vapor pressure and, consequently, the flux will increase [17]. The only exception from this rule is when the increase of feed temperature causes the temperature polarization and weakens the vapor flux.

For the analysis of the effect of feed temperature on the permeate flux, the range of 45–75°C has been used in this study with the water/glucose syrup as the inlet feed. The experimental and simulated permeate flux in the mentioned temperature range has been plotted in Fig. 5.

As it was expected, both the experimental and simulated results follow the exponential trend known as Antoine equation. The increase in the inlet feed temperature yields to increase in the vapor pressure of the feed and consequently, the compressibility of the water in the liquid phase (Z_l) increases significantly while the compressibility factor of the water in the gas phase (Z_v) decreases slowly and as a result, the constant factor, λ, decreases. Decline in the quantity of the factor λ shows that at the constant feed concentration, the concentration of the permeant in the gas phase will be more. When the concentration of the permeant in the gas phase increases, the driving force for diffusion of the water molecules through the membrane increases and the flux enhances correspondingly. As it can be seen from Fig. 5, the simulated results have the rational agreement with the experimental results. The Peng–Robinson cubic equation of state has the best concurrence with the experimental results among the three studied equations, while the other two equations' data lay above the data got from the PR equation. Moreover, the exponential trends have been kept better in the simulated results than the experimental results and this may show some errors made by the experiments or experimenters. The temperature drop across the membrane increases at higher temperatures by evaporative cooling that occurs at the permeate section [16]. This phenomenon decreases the temperature across the membrane and has made us unable to calculate the exact temperature on the membrane surface. At the higher temperatures, this temperature drop will be more and as a consequence, the deviance between the experimental and simulated data increases.

3.3. Effect of feed concentration

Increasing the feed concentration will result in vapor pressure drop which will yield to some reduction in the permeate flux. Obtained experimental

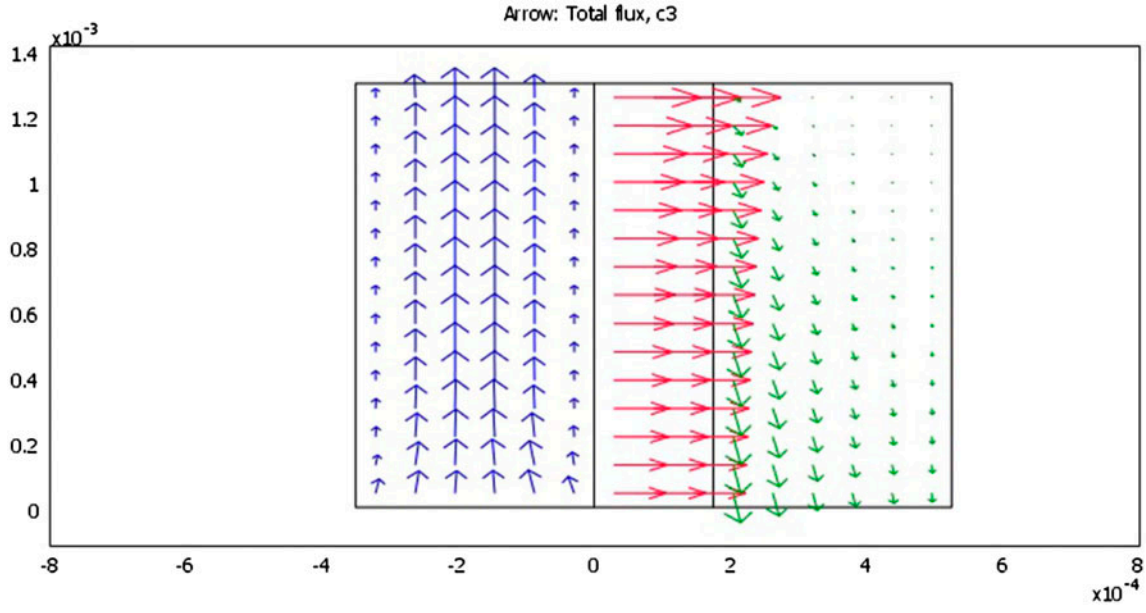

Fig. 4. Permeant flux arrow plot in the studied domain.

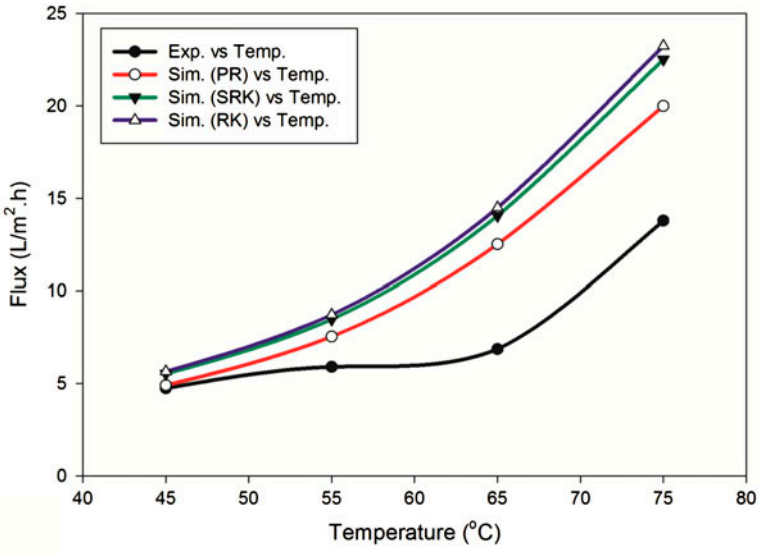

Fig. 5. Effect of inlet feed temperature on the experimental and simulated flux.

results and simulated results by three cubic equations of state under the concentration range of 10–150 g/L of glucose in the water/glucose syrup have been plotted in Fig. 6. As can be seen, by increasing the temperature, the experimental flux decreases from 6.66 to 3.38 g/L, while the simulated fluxes are nearly constant in the mentioned range of concentration. Based on the proposed cubic equations of state, vapor pressure has significant effect on the flux, but vapor pressure alteration under the studied feed concentrations is negligible. It is worth mentioning that we cannot expect to have significant changes in vapor pressure until high glucose concentrations like 1,000 g/L based on the vapor pressure data. However, the real conditions are more different from modeling and simulation, and the membrane fouling and temperature polarization increase as the concentration increases and they yield to lower fluxes [18,19].

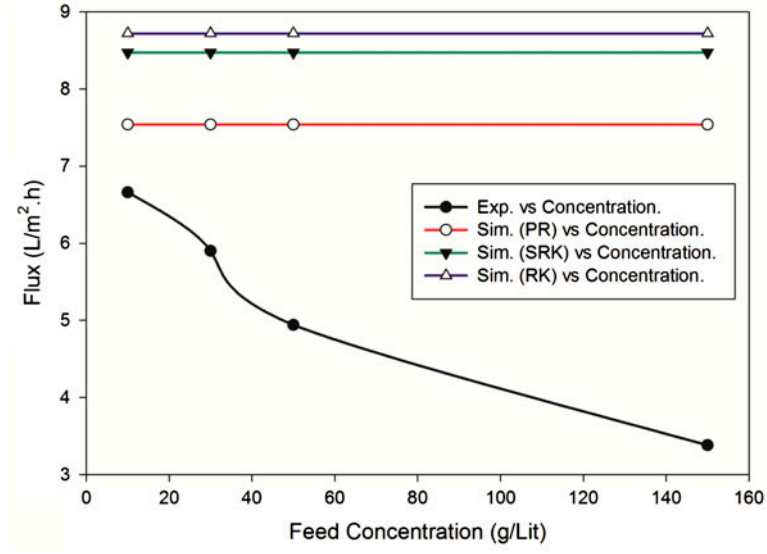

Fig. 6. Effect of feed concentration on the experimental and simulated flux.

3.4. Effect of feed flow rate

By increasing the feed flow rate, the feed temperature will enhance which in return yields to increase of feed vapor pressure [20]. As it was discussed before, the mass transfer driving force increases by the vapor pressure and so, the permeate flux increases. In this study, the effect of feed flow rate on the permeate flux has been studied and selected range includes the feed flow rate of 200–600 ml/min. The experimental and simulated results have been shown in Fig. 7. As can be seen by increasing the feed flow rates in both of the experimental and simulated results, the flux increases but the deviation from the simulated and experimental results is more in higher velocities. This deviation can be explained by the fact that at higher temperatures, temperature drop is more significant rather than lower temperatures and lower velocities. From the experimental view, when the feed flow rate increases from 200 to 600 ml/min, the decrease in boundary layer resistance minimizes the concentration polarization and so, the flux increases [21]. In the simulation procedure, the most important effect of the feed flow rate is on the factor λ which relates the permeant concentration in the liquid and gas phase. So, by increasing the feed flow rate, the factor λ decreases and the permeate flux increases. It is worth mentioning that all of three generic cubic equations are able to model the experimental results to some extent.

3.5. Effect of sweeping gas flow rate

The increase in the sweeping gas flow rate maintains the turbulence and Reynolds number at high levels which results in changing the hydrodynamics conditions in the permeate side and decreasing the temperature polarization adjacent to the membrane in the permeate section. At the other side, by increasing the sweeping gas flow rate, the vapor pressure in the permeate section decreases and so, the mass transfer and permeant flux through the membrane increases [22,23]. The results of the effect of sweeping gas flow rate in the range of 4–16 SCFH on the permeate flux have been plotted in Fig. 8. As can be seen, the effect of sweeping gas flow rate on the permeate flux is more than what was achieved due to the change in the feed flow rate. By increasing the sweeping gas flow rate, the flux in both of the experimental and simulated results increases which admits that the mass transfer driving force increases at higher velocities. The ascendant trend in the simulated results are more sharper than the experimental results and this can be explained in this way that there are still some resistance and temperature polarization at these levels of velocities which the models are unable to predict.

For better understanding of the effect of sweeping gas flow rate on the permeate flux, the surface plot of the total flux in the permeate section under three different sweeping gas flow rates has been plotted (Fig. 9). As it is clear, when the sweeping gas flows from upward to downward in the permeate section, it sweeps the permeant molecules, and more the velocity of the sweeping gas, more molecules are transferred at the constant conditions. The parabolic curve in the plots that resembles the mass boundary layer is more visible at higher flow rates.

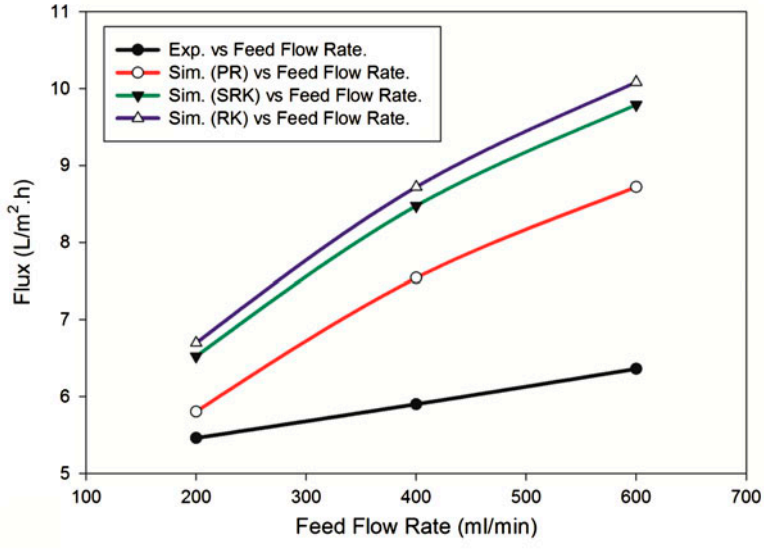

Fig. 7. Effect of feed flow rate on the experimental and simulated flux.

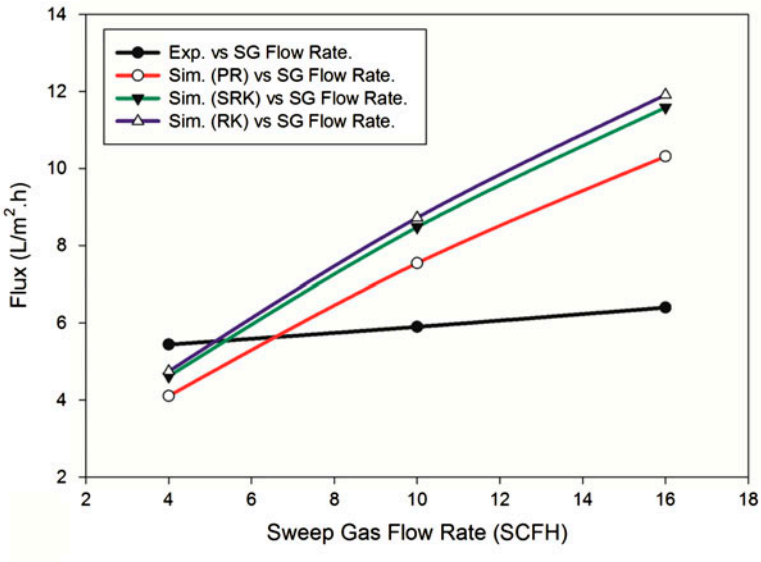

Fig. 8. Effect of sweeping gas flow rate on the experimental and simulated flux.

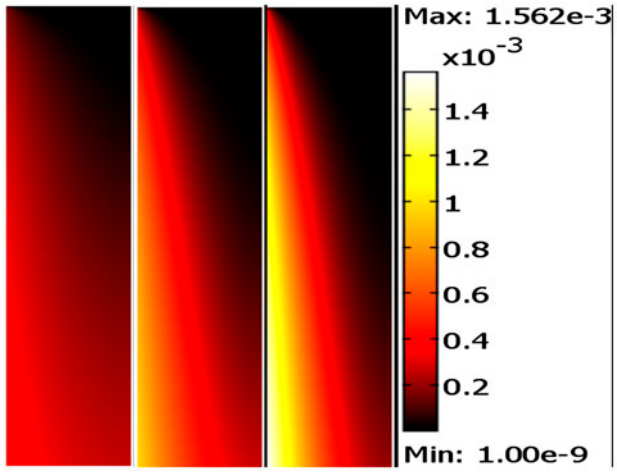

Fig. 9. Surface plot of the total flux under different velocities.

4. Conclusion

In this article, a two-dimensional model has been used for modeling the feed, membrane, and permeates section in the separation of water/glucose syrup by micro porous PTFE MD. The conservation equations in these three sections have been derived and solved by COMSOL Multiphysics which uses the proven FEM. Peng–Robison, Redlich–Kwong, and Soave–Redlich–Kwong cubic equations of state were used in the modeling procedure to make bridge between the water concentrations at two different sides of the membrane. Obtained simulation results show that Peng–Robinson is more powerful in modeling the experimental results than the other two equations. Simulated results laid above the experimental results because of the evaporative cooling occurred at the permeate section and caused the temperature drop along the membrane module. Obtained simulated permeate flux increased with the temperate increase and it followed the exponential trend that looks like what can be obtained by the Antoine equation, because of the increase in the quantity of factor λ. Simulated results were unable to model the effects of glucose concentration due to membrane fouling and temperature polarization at high glucose concentrations. The effect of feed flow rate and sweeping gas flow rate increase was in the raise of both of the experimental and simulated results, while the changes based on the second one were more at the studied ranges of flow rates. The proposed modeling procedure is able to model the sweeping gas MD performance whose major use is in desalination and water purification.

Nomenclature

C_W	—	water concentration
t	—	time
R_W	—	chemical reaction
J_W	—	diffusive molar flux
D_W	—	diffusion coefficient
V	—	velocity vector
ρ	—	density
P	—	pressure

g — gravity
C_{Wf} — water concentration in the feed section
C_{Wm} — vapor concentration in the membrane section
Z_l — water compressibility factor in the liquid phase
Z_v — water compressibility factor in the gas phase
v — molar volume
P_r — reduced pressure
T_r — reduced temperature
q — dimensionless constant
T — temperature
v_l — water molar volume in the liquid phase
v_g — water molar volume in the gas phase
A_W — dimensional quantity for water
A_G — dimensional quantity for glucose
B_W — constant
B_G — constant
C_{Wp} — vapor concentration in the permeate section
q — mesh quality
A — area
h_1, h_2, h_3 — lengths of the triangular

Greek symbols

λ — partition coefficient
μ — dynamic viscosity
β — dimensionless constant
ε — dimensionless constant
σ — dimensionless constant
Ω — dimensionless constant
Ψ — dimensionless constant
ω — acentric factor

References

[1] A. Alkhudhiri, N. Darwish, N. Hilal, Membrane distillation: A comprehensive review, Desalination 287 (2012) 2–18.
[2] M. Essalhi, M. Khayet, Application of a porous composite hydrophobic/hydrophilic membrane in desalination by air gap and liquid gap membrane distillation: A comparative study, Sep. Purif. Technol. 133 (2014) 176–186.
[3] J. Minier-Matar, A. Hussain, A. Janson, F. Benyahia, S. Adham, Field evaluation of membrane distillation technologies for desalination of highly saline brines, Desalination 351 (2014) 101–108.
[4] S. Shirazian, S.N. Ashrafizadeh, Near-critical extraction of the fermentation products by membrane contactors: A mass transfer simulation, Ind. Eng. Chem. Res. 50(4) (2011) 2245–2253.
[5] S. Shirazian, A. Moghadassi, S. Moradi, Numerical simulation of mass transfer in gas–liquid hollow fiber membrane contactors for laminar flow conditions, Simul. Model. Pract. Theory 17(4) (2009) 708–718.
[6] S. Shirazian, A. Marjani, F. Fadaei, Supercritical extraction of organic solutes from aqueous solutions by means of membrane contactors: CFD simulation, Desalination 277(1–3) (2011) 135–140.
[7] M. Rezakazemi, M. Shahverdi, S. Shirazian, T. Mohammadi, A. Pak, CFD simulation of water removal from water/ethylene glycol mixtures by pervaporation, Chem. Eng. J. 168(1) (2011) 60–67.
[8] R.B. Bird, W.E. Stewart, E.N. Lightfoot, Transport Phenomena, John Wiley & Sons, New York, NY, 2006.
[9] M. Khayet, Membranes and theoretical modeling of membrane distillation: A review, Adv. Colloid Interface Sci. 164(1–2) (2011) 56–88.
[10] M.M.A. Shirazi, L. Fatehi, D. Bastani, A. Kargari, M. Soleimani, M.J.A. Shirazi, Application of sweeping gas membrane distillation for concentration of glucose syrup, Seventh International Chemical Engineering Congress and Exhibition, Kish, Iran, November 2011, pp. 21–24.
[11] J.H. Perry, Chemical engineers' handbook, J. Chem. Edu. 27(9) (1950) 533.
[12] J.M. Smith, H.V. Ness, Introduction to Chemical Engineering Thermodynamics, McGraw-Hill, New York, NY, 2011.
[13] A. Converti, M. Zilli, S. Arni, R. Di Felice, M. Del Borghi, Estimation of viscosity of highly viscous fermentation media containing one or more solutes, Biochem. Eng. J. 4(1) (1999) 81–85.
[14] S. Glasstone, K.J. Laidler, H. Eyring, The theory of rate processes: The kinetics of chemical reactions, viscosity, diffusion and electrochemical phenomena, McGraw-Hill Book Company, New York, NY, 1941.
[15] K. Malek, M.O. Coppens, Knudsen self- and Fickian diffusion in rough nanoporous media, J. Chem. Phys. 119 (2003) 2801–2811.
[16] D. O'Brien, J. Craig Jr., Ethanol production in a continuous fermentation/membrane pervaporation system, Appl. Microbiol. Biotechnol. 44(6) (1996) 699–704.
[17] M. Khayet, P. Godino, J.I. Mengual, Theory and experiments on sweeping gas membrane distillation, J. Membr. Sci. 165(2) (2000) 261–272.
[18] L. Martínez, Comparison of membrane distillation performance using different feeds, Desalination 168 (2004) 359–365.
[19] L. Martínez-Díez, M.I. Vázquez-González, Temperature and concentration polarization in membrane distillation of aqueous salt solutions, J. Membr. Sci. 156 (2) (1999) 265–273.
[20] N. Tang, H. Zhang, W. Wang, Computational fluid dynamics numerical simulation of vacuum membrane distillation for aqueous NaCl solution, Desalination 274(1–3) (2011) 120–129.
[21] S. Srisurichan, R. Jiraratananon, A. Fane, Mass transfer mechanisms and transport resistances in direct contact membrane distillation process, J. Membr. Sci. 277(1–2) (2006) 186–194.
[22] M.M.A. Shirazi, A. Kargari, M.J.A. Shirazi, Direct contact membrane distillation for seawater desalination, Desalin. Water Treat. 49(1–3) (2012) 368–375.
[23] K. Charfi, M. Khayet, M. Safi, Numerical simulation and experimental studies on heat and mass transfer using sweeping gas membrane distillation, Desalination 259(1–3) (2010) 84–96.